Supplemental Figures

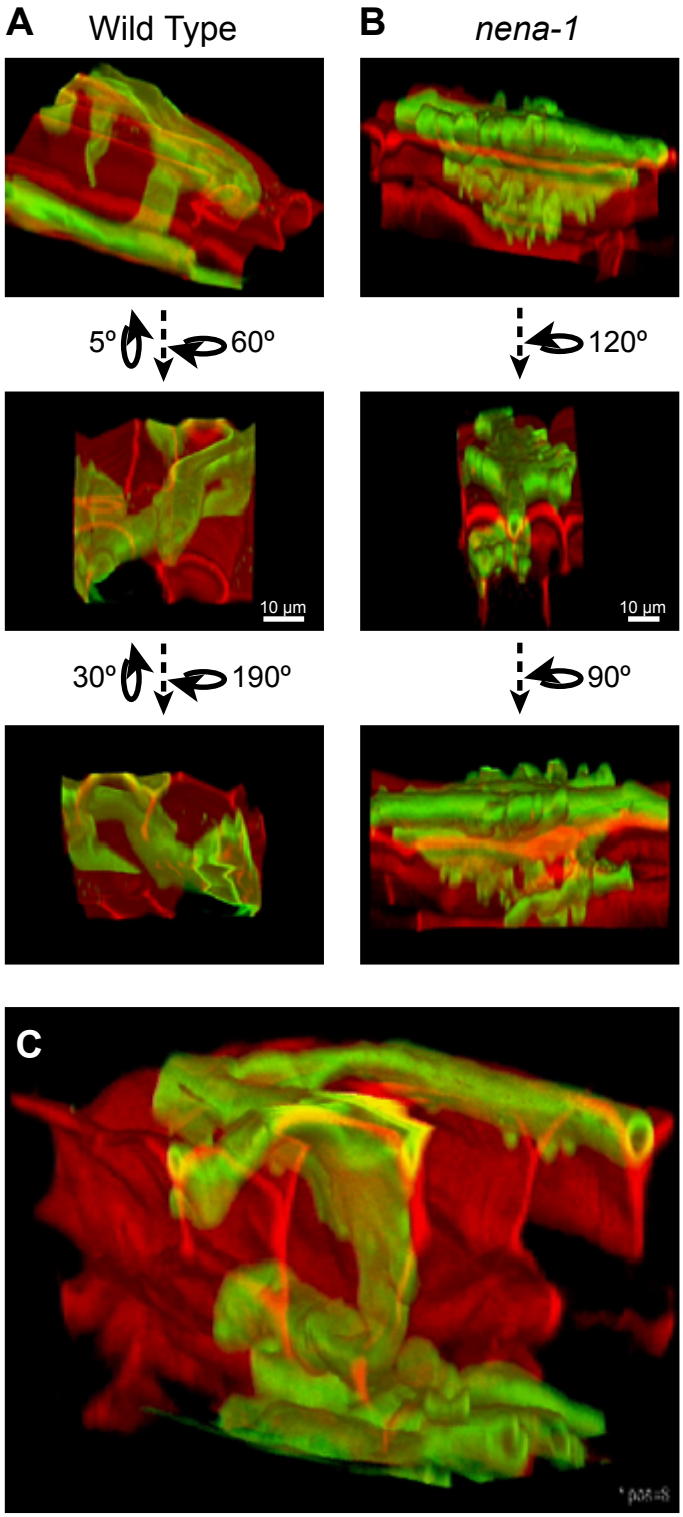

Supplemental Figure 1. 3D Projection of Typical AM Infection Sites in Wild Type and *nena-1*.
(A) to **(C)** Fungal (green) and plant cell wall (red) structures were stained with WGA-Alexa Fluor 488 and propidium iodide, respectively. Structures were imaged by CLSM and are illustrated from different relative angles, as indicated. In WT (A), a tubular hypha branches perpendicular from a surface 'runner' hypha and transversally penetrates a rhizodermal cell before diverging inside the root. In *nena-1* (B), a 'runner' hypha penetrates the root surface between rhizodermal cells and forms excessive swellings; infection is aborted at the subepidermal layer. (C) Successful penetration of the rhizodermis in *nena-1* is accompanied by hyphal deformations.

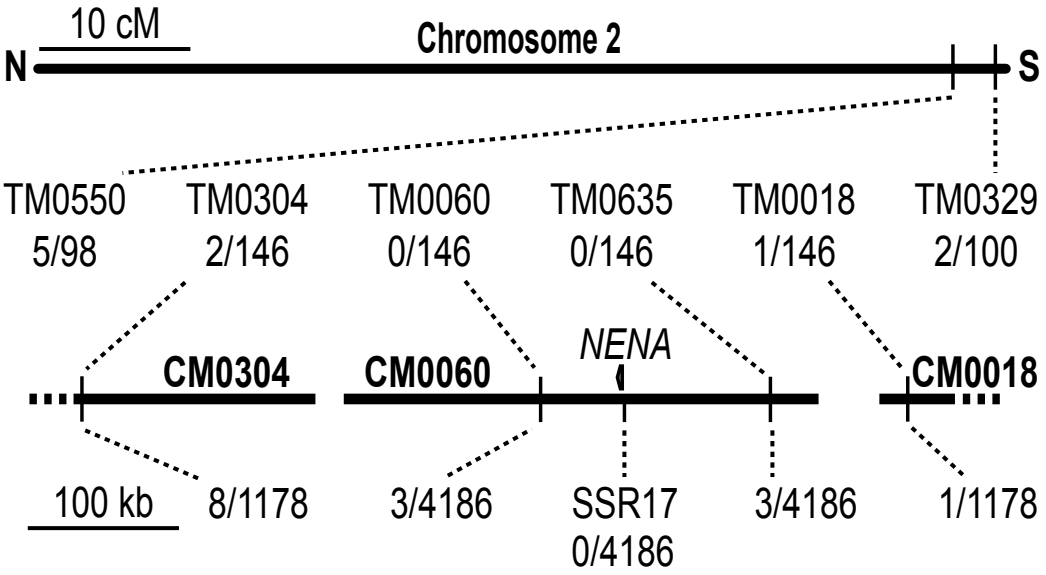

Supplemental Figure 2. Map-Based Cloning of *NENA*.
Genetic map of chromosome 2 (top) and physical map of contigs CM0304 and CM0018 encompassing CM0060 incl. the *NENA* locus (bottom). Positions and names of co-segregating SSR markers and the *NENA* gene are indicated. Ratios are numbers of recombinant/non-recombinant alleles of respective markers in *nena-1* x MG20 F2 sub-populations. Marker names (except SSR17) and distances accord to the *Lotus* genome project.

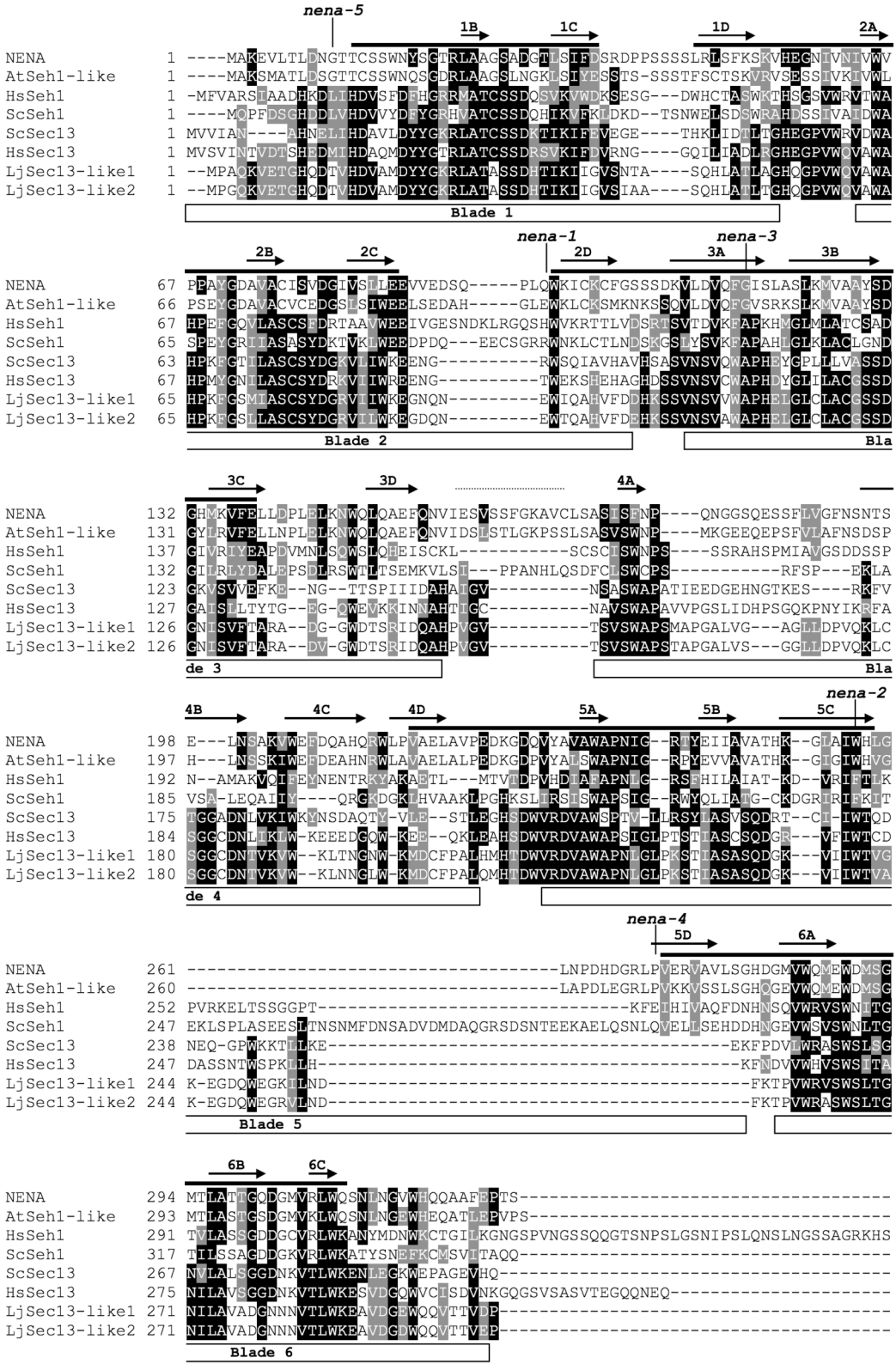

Supplemental Figure 3. Alignment of Seh1 and Sec13 Related Protein Sequences from *L. japonicus*, *A. thaliana*, *H. sapiens* and *S. cerevisiae*. (Figure legend continues on next page.)

(Supplemental Figure 3, continued:) Residues that are identical or similar to the consensus sequence (≥ 50 % similarities) are inverted or highlighted in gray background, respectively. The secondary structure corresponding to the 3D model of NENA (Figure 5C) is indicated as arrows (β strands, labels refer to blade number and strand order) or dotted line (helix) above the alignment. WD40 repeats that were predicted from the NENA sequence are marked as black lines above the alignment. Boxes under the alignment represent β-propeller blades of yeast Seh1 (Brohawn et al., 2008). Mutated residues of respective alleles are indicated above the alignment. Protein accessions are given in Supplemental Figure 4.

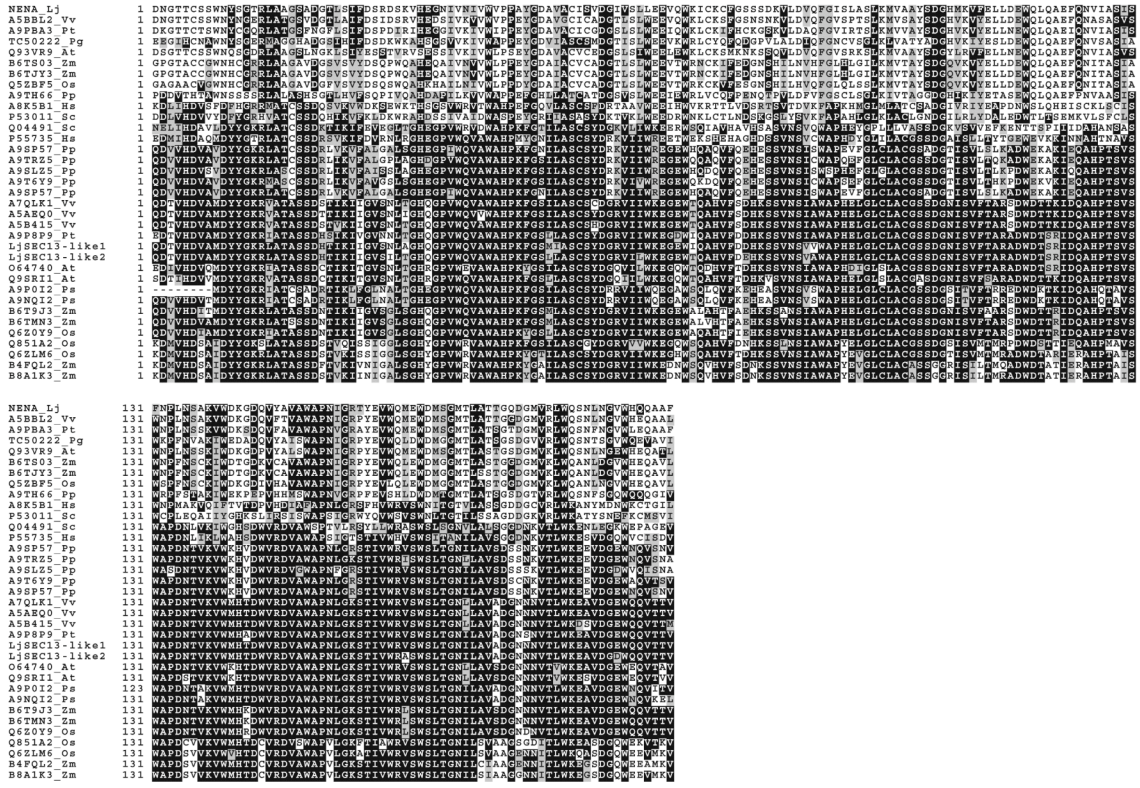

Supplemental Figure 4. Multi-Species Alignment of Seh1 and Sec13 Related Proteins.
Residues that are identical or similar to the consensus sequence (≥ 30 % similarities) are inverted or highlighted in gray background, respectively. Blocks containing gaps or poorly conserved sequences have been masked. The presented alignment was used to generate the phylogenetic tree in Figure 4. GenBank/UniProt accessions and species acronyms are indicated left to the sequences.

A

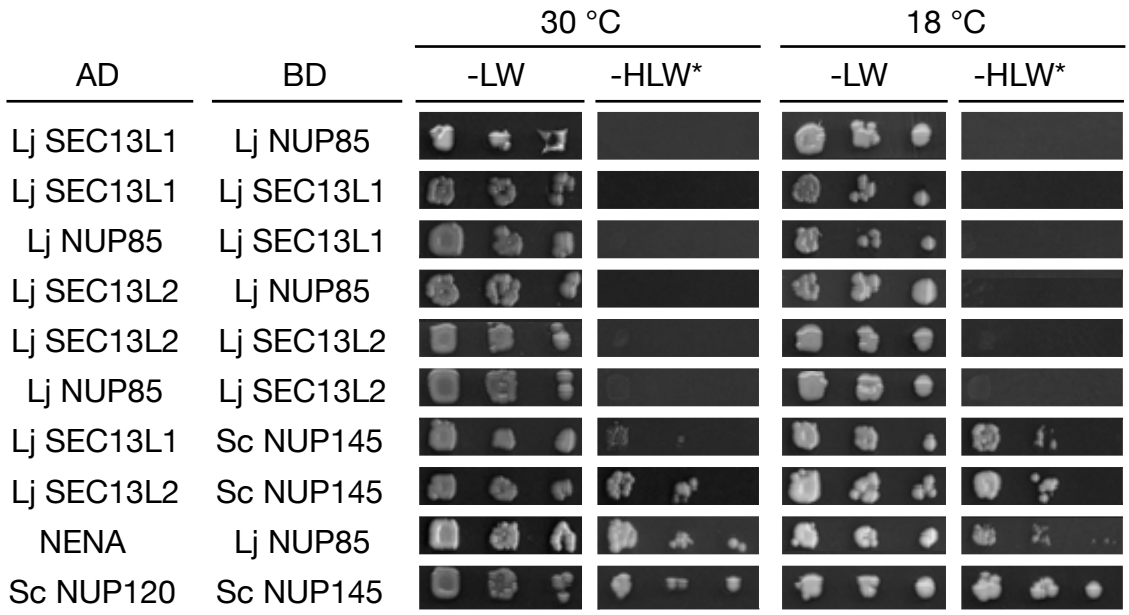

B

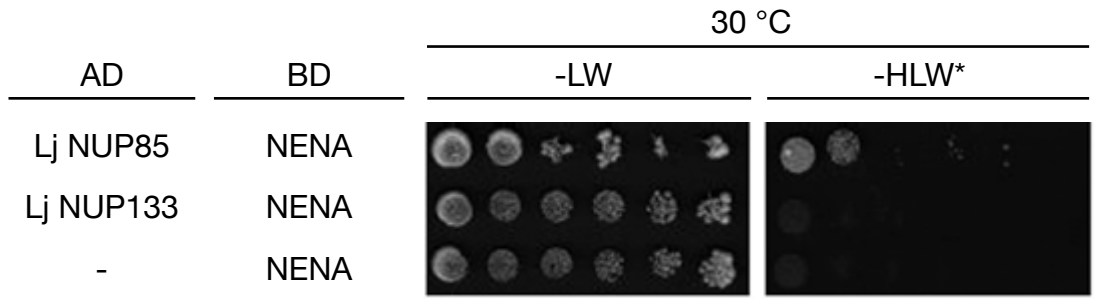

Supplemental Figure 5. In Contrast to NENA, SEC13-like 1 and SEC13-like 2 Do Not Interact with NUP85 in the Gal4-Based Yeast Two-Hybrid Assay.

(A) and **(B)** Prey (AD) and bait (BD) contructs were co-transformed and yeast was grown in 3 (A) or 5 (B) dilutions on synthetic dropout medium lacking leucine and tryptophan (-LW) or histidine, leucine and tryptophan (-HLW) supplemented with 15 mM 3-amino-1,2,4-triazole (*). (A) In order to test for temperature dependent interaction, the assay has been carried out at 30 °C and 18 °C. (B) NENA and NUP85 interact in both prey and bait combinations (see Figure 5A). (-) Bait vector containing the Gateway reading frame cassette including *ccdB* and Cm^R.

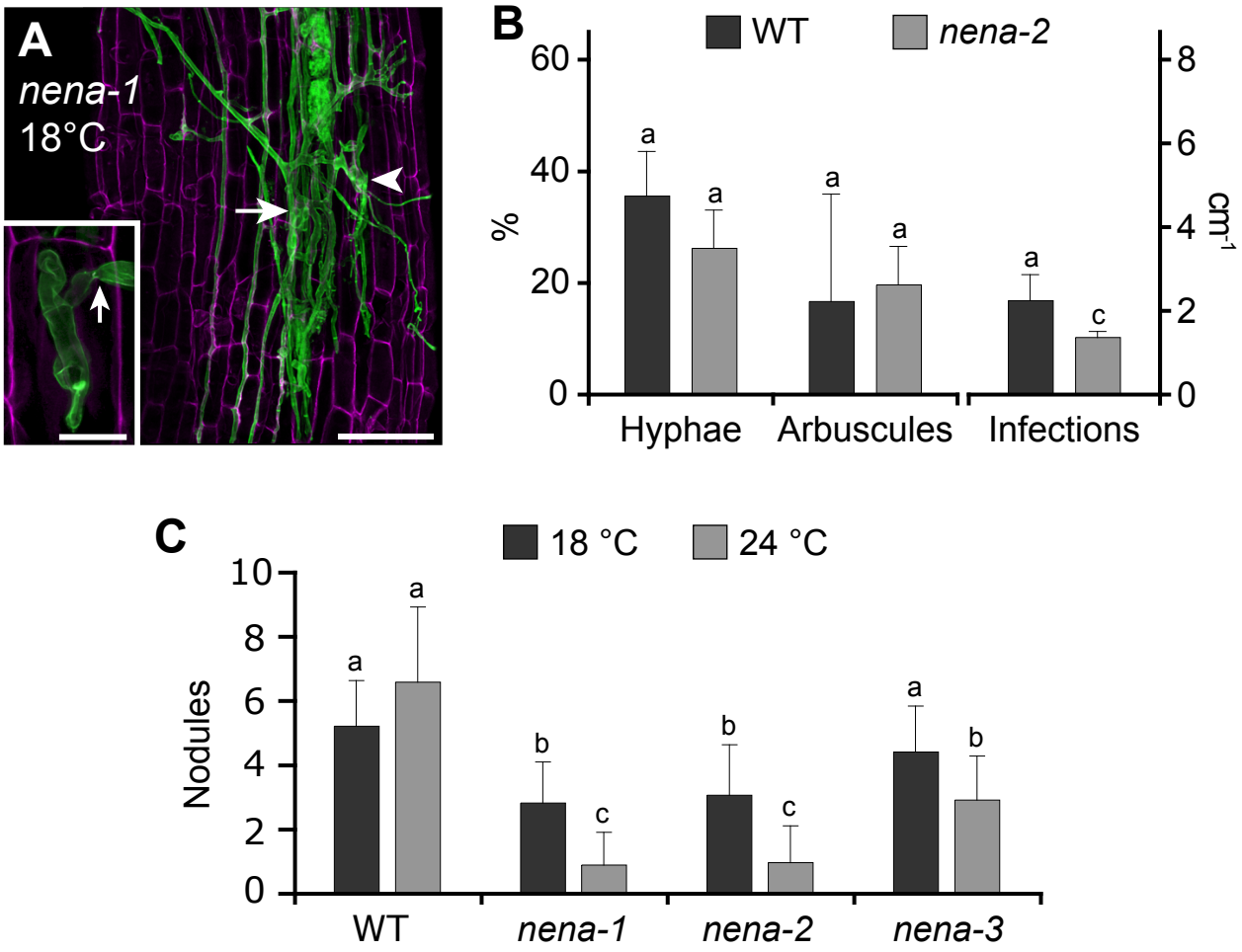

Supplemental Figure 6. AM and Nodulation Defects of *nena* Are Temperature Dependent.
(A) Confocal z-projection of AM structures (green) in *nena-1* co-cultivated with BEG195 for 3 weeks at 18 °C. Arrows and arrowheads indicate successful and aborted infection events, respectively. Inset shows an infection site at higher magnification. Scale bars: 100 µm, inset 20 µm.
(B) Mean hyphal colonization (Hyphae, %), arbuscular colonization (Arbuscules, %) per root and mean successful infection sites per cm per root (Infections) from WT and *nena-2* plants (n≥4) after 3 weeks of cultivation at 18 °C. Error bars show SD. Different letters above bars indicate significant differences (p≤ 0.05, *t*-test) between pair wise comparisons.
(C) Average nodule numbers at 18 °C vs. 24 °C growth temperature on WT and *nena* individuals (n≥10). *nena* formed less nodules at 24 °C than at 18 °C and, except for *nena-3* at 18 °C, nodulation was reduced in *nena* compared to WT. Error bars show SD. Different letters above bars indicate significant differences (p≤0.05, *t*-test) between pair wise comparisons.

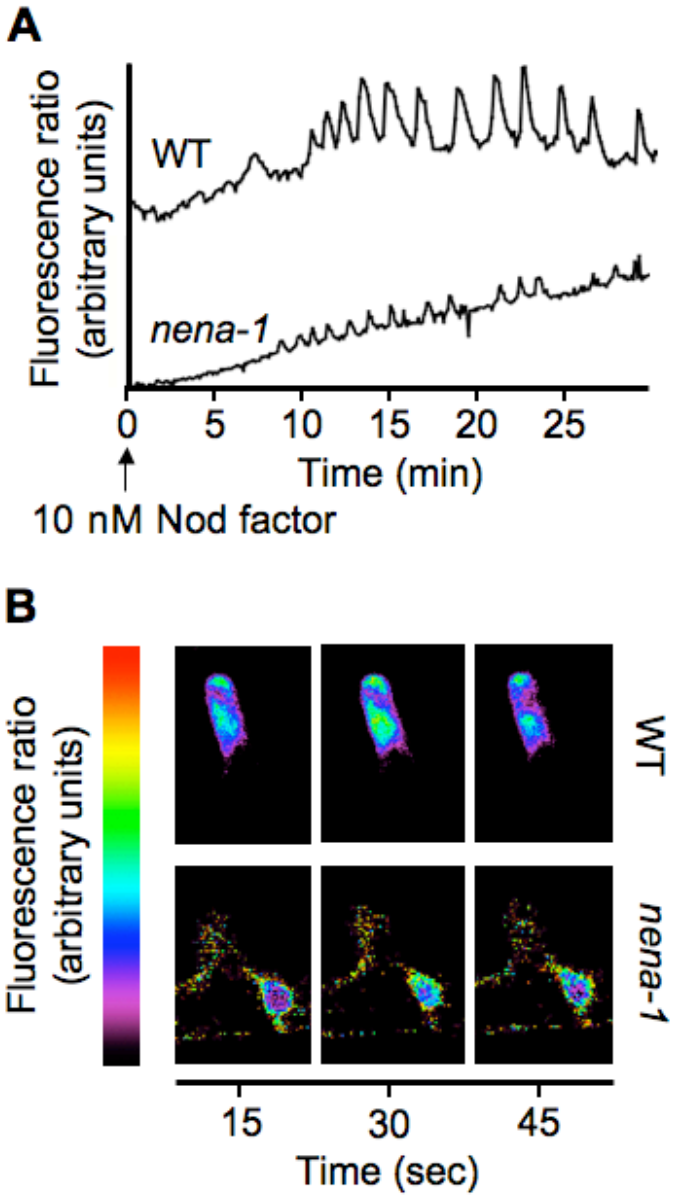

Supplemental Figure 7. Calcium Spiking in Root Hairs of Wild Type and *nena-1.*
(A) Fluorescence ratios between ratiometric Ca^{2+} indicator Oregon Green 488 BAPTA-1 (OG) and reference dye Texas Red (TR) after NF application to roots are indicated over time. The upper trace is representative of positive spiking in *L. japonicus* Gifu wild type. The lower trace represents an exceptional positive spiking in *nena-1.*
(B) Images of one Ca^{2+} spike before (15 sec time point), during (30 sec) and after (45 sec) a perinuclear Ca^{2+} burst in a WT root hair and a *nena-1* trichoblast. False colors represent fluorescence ratios between OG and TR.

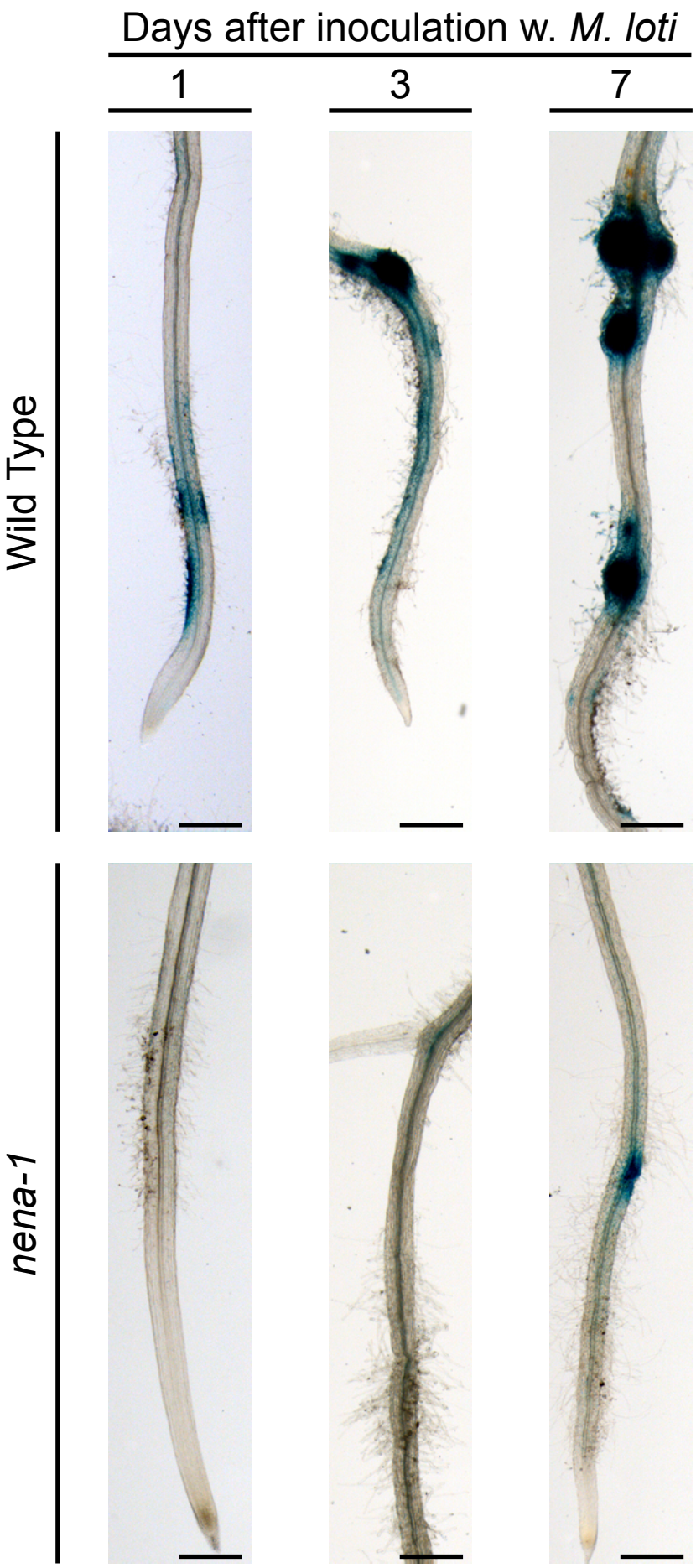

Supplemental Figure 8. The *NIN* Promoter Is Not Induced During Early Rhizodermal Response to *M. loti* but Active During Nodule Formation in *nena-1*.

Brightfield images of X-Gluc incubated roots transformed with *GUS*-reporter fused to the promoter of *NIN*. No blue rhizodermal staining was observed in *nena-1* roots at 1 and 3 dpi. Images represent observations given in Table 3. Scale bars: 0.5 mm.

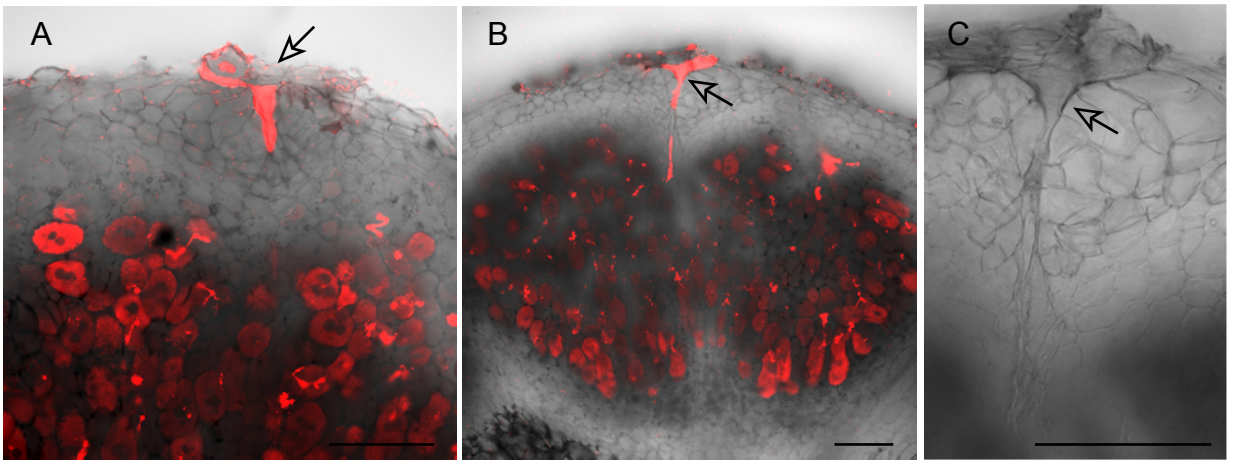

Supplemental Figure 9. Intercellular Infection of Outer Nodule Cell Layers in *nena-1*.
(A) to **(C)** Confocal z-projections of 80 µm longitudinal tissue sections showing intercellular infection (arrows) and cortical cell colonization by DsRed expressing *M. loti* (red). (C) Shows the infection site in (B) at higher magnification in brightfield (BF) channel only. (A) and (B) are overlays of RFP and BF channels. Images represent samples from 21 dpi/waterlogged+5 µM AVG treatments. Scale bars: 100 µm.

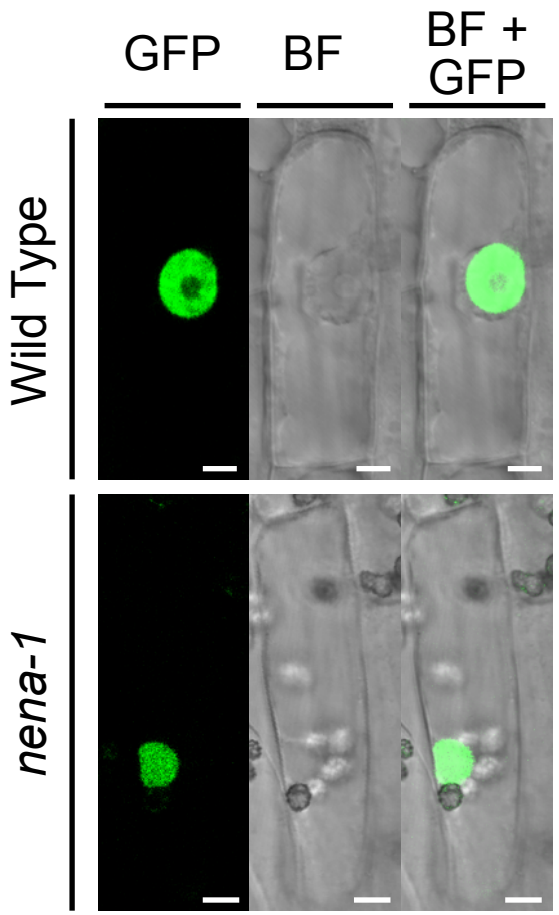

Supplemental Figure 10. GFP-Cyclops Localizes to the Nucleus in *nena-1*.
Confocal micrographs of *A. rhizogenes* transformed root cells in GFP, bright field (BF) and overlayed channels. No difference in localization of the GFP signal was detected between transgenic roots in WT and *nena-1* backgrounds. Scale bars: 5 µm.

Supplemental Tables

Supplemental Table 1. *nena* Alleles and Symbiotic Phenotypes

Allele	Line	Mutation	Nodulation	AM[a]
nena-1	SL1839-1, SL1841-N	Q97Stop	-, t.s.	+/-, t.s.
nena-2	SL0181-1	W257Stop	-, t.s.	+/-, t.s.
nena-3	SL1546-1	G117E	+/-, t.s.	n.d.
nena-4	SL0703-1	P270S	+	n.d.
nena-5	SL1747-1	G11S	+	n.d.
nena-6	C1978	Del./Inversion*	-**	-**

[a], hyphal colonization; -, significantly reduced at 24°C and 18°C; +/-, significantly reduced at 24 °C only; +, wild type-like; t.s., temperature sensitive, significantly lower symbiotic performance at 24 °C vs. 18 °C; *, *NENA* disruption by chromosomal rearrangements from C^{6+} irradiation of MG-20; **, determined at 22 °C only; n.d., not determined.

Supplemental Table 2. Primers Used in this Work

Primer Name	Use/Target	Direction	Sequence
TM0550-KS	Map-based cloning; forward primers contain 5' tails for fluorescent labeling	Forward	5'-TCGAGGTCGACGGTATCCCTGTTGGCTTATCTTAGTATG-3'
		Reverse	5'-AAAACAAGTGGAAGTGAGTTAG-3'
TM0304-LUF		Forward	5'-CTCGTAGACTGCGTACCACGTTCTCTGGGAACTTATGAC-3'
		Reverse	5'-ATTTGTTGTGTGCACTCAGG-3'
TM0060-KS		Forward	5'-TCGAGGTCGACGGTATCTCAAGTGGGAGTAAGTTAGCATTCC-3'
		Reverse	5'-ATGGTTGGATAATAGACTTAGCCGA-3'
TM0635-M13		Forward	5'-GTAAAACGACGGCCAGTTTAATCCACCACCCTGACCG-3'
		Reverse	5'-ATAACCCTCCTCAAACATCG-3'
TM0018-BKRSV		Forward	5'-CGCCATTTGACCATTCAGTTTGAGCAAGTTAGAGGTG-3'
		Reverse	5'-CGGATAAGAAAGGTAGAAGAG-3'
SSR17-BKRSV		Forward	5'-CGCCATTTGACCATTCAGTACCGGAGTAGTTCCAGGATG-3'
		Reverse	5'-GCTACTGTTAAACCCCGGAAAC-3'
FAM-LUF	3'-fluorescent labeled universal primer for map-based cloning	Forward	5'-CTCGTAGACTGCGTACCA-3'
VIC-BKRSV		Forward	5'-CGCCATTTGACCATTCA-3'
NED-KS		Forward	5'-TCGAGGTCGACGGTATC-3'
PET-M13		Forward	5'-GTAAAACGACGGCCAGT-3'
TM0329	Map-based cloning	Forward	5'-TGGGTGAGAATCTCAGAGGG-3'
		Reverse	5'-ATCCAATCCATTCCTTTCTG-3'
N-166	TILLING/*NENA*	Forward	5'-AAGTTAGAATTTATAAGGGCATCATT-3'
N-167		Reverse	5'-GGATTCCTGGCTTCCACCATTTTGTG-3'
N-156		Forward	5'-CCAGCTTGCTTTTACCTATTGGTCAT-3'
N-157		Reverse	5'-GCGCCAGCTTACTACTTACAAGTTA-3'
N-172	Transgenic complementation and sub-cellular localization/ *NENA*	Forward	5'-CAGCAAATCCACCACCACTAGTTAC-3'
N-157		Reverse	5'-GCGCCAGCTTACTACTTACAAGTTA-3'
N-171		Forward	5'-CACCGGAAAATTACACAAAAGATGGT-3'
N-168		Reverse	5'-AGAAGTGGGTTCAAATGCAGCCT-3'
N-171		Forward	5'-CACCGGAAAATTACACAAAAGATGGT-3'
N-173		Reverse	5'-CTCTCGTGAAACCTAAAATCTTG-3'
N-158		Forward	5'-CACCATGGCGAAGGAGGTGTTGAC-3'
N-168		Reverse	5'-AGAAGTGGGTTCAAATGCAGCCT-3'
S-176	Transgenic complementation/ *AtSeh1L*	Forward	5'-ATATTTTGGCCCAAGTCTTGATAAT-3'
S-175		Reverse	5'-ACTGTCAAATAGTGTGTGGGAAATG-3'
S-177		Forward	5'-ATGGCGAAATCAATGGCGACG-3'
S-178		Reverse	5'-TTAGGAGGGAACTGGTTCAAG-3'
N-179	Transg. compl./*pENTR-NENA*	Reverse	5'-AAGGGTGGGCGCGCCGAC-3'
N-158	Y2H analysis/*NENA*	Forward	5'-CACCATGGCGAAGGAGGTGTTGAC-3'
N-159		Reverse	5'-CTAAGAAGTGGGTTCAAATGCAG-3'
85-162	Y2H analysis and sub-cellular localization/*NUP85*	Forward	5'-CACCATGCCCTCCGACACAGTC-3'
85-163		Reverse	5'-CTATTCATCAAGTATAGCACGACC-3'
85-183		Reverse	5'-TTCATCAAGTATAGCACGACCA-3'
133-160	Y2H analysis/*NUP133*	Forward	5'-CACCATGTTTTCGTGTGGAACGAAGAAG-3'
133-161		Reverse	5'-CTATTCCATGGGAGAAGGCCCT-3'
13-1-191	Y2H analysis/*SEC13-1*	Forward	5'-CACCATGCCTGCTCAGAAGGTTGAAACG-3'
13-1-194		Reverse	5'-CTACGGATCCACTGTTGTCACCTGTTGCCAT-3'
13-1-195		Forward	5'-CGTTTACACTCACCGGCGACT-3'
13-1-196		Reverse	5'-TGCATTGTGAAGCACAGGTAA-3'
13-1-192	Y2H analysis/*SEC13-2*	Forward	5'-CACCATGCCTGGTCAAAAGGTTGAAACA-3'
13-1-193		Reverse	5'-CTACGGTTCCACAGTCGTCACCTGTTGCCAG-3'
13-1-197		Forward	5'-CCTCACACGGTTGACACCACA-3'
13-1-198		Reverse	5'-CTCGTAAGCACAGAATGTTCAGT-3'
120-5'	Y2H analysis/*ScNup120*	Forward	5'-CACCATGGCATGCCTCTCAAGAATTGATG-3'
120-3'		Reverse	5'-CTATAGACCTCGTAACTCATCTCT-3'
145-5'	Y2H analysis/*ScNup145*	Forward	5'-CACCATGTTTAATAAAAGTGTAAATAGTG-3'
145-3'		Reverse	5'-TTATATCTTATATGTACACTTCATTA-3'
N-174	Expression analysis/*NENA*	Forward	5'-AACTGGCAACTTCAGGCTGAGTTTC-3'
N-167		Reverse	5'-GGATTCCTGGCTTCCACCATTTTGTG-3'
EF1-U23	Expression analysis/*EF-1 α*	Forward	5'-GCAGGTCTTTGTGTCAAGTCTT-3'
EF1-L19		Reverse	5'-CGATCCAGAACCCAGTTCT-3'
NIN-201	Expression analysis/*NIN*	Forward	5'-TGGATCAGCTAGCATGGAAT-3'
NIN-202		Reverse	5'-TCTGCTTCTGCTGTTGTCAC-3'
M4-199	Expression analysis/*SbtM4*	Forward	5'-TCTCATAGTTGCGGCACCAC-3'
M4-200		Reverse	5'-TGTCTTATTACCCAACCCTGTGC-3'
SbtS-007	Expression analysis/*SbtS*	Forward	5'-ATTGATCACAATGCCAGAGATG-3'
SbtS-008		Reverse	5'-TGTTGGGAAGATTGTAGCAGTG-3'
40-203	Expression analysis/*ENOD40-1*	Forward	5'-CCTCTGAACCAATCCATCAAATCCA-3'
40-204		Reverse	5'-AGGAGTGTGAGAGGTGACAGCA-3'

Supplemental Methods

Map-Based Cloning

AM phenotypes of 276 F2 self-progeny from MG-20 x *nena-1* (SL1841-N, M3 mutant J8690) were determined (see AM mutant screen), genomic DNA was isolated and scanned for co-segregation with SSR markers. Primer sequences and marker information were retrieved from the miyakogusa.jp website (http://www.kazusa.or.jp/lotus/). Within the scored F_2 individuals, the allelic distribution of 30 SSR markers evenly covering the six chromosomes of *L. japonicus* displayed co-segregation of Gifu alleles with the mutant phenotype at the south end of linkage group two, between SSR markers TM0550 and TM0329 (Supplemental Figure 2, top). After delimiting the location of *NENA* to a 0.4 cM interval on the south end of linkage group two, co-segregating markers were positioned on a physical contig of transformation-competent artificial chromosomes clones that were completely sequenced in the context of the *Lotus* genome project (Supplemental Figure 2, bottom). Additional markers were derived from the contig sequence and used for identification of recombination events between markers flanking the target region. 2093 F2 individuals were genotyped by DNA isolation from 2 weeks old seedlings, followed by fluorescent labeling (Schuelke, 2000) of PCR amplified SSR markers TM0304 and TM0018 flanking the *nena* locus. AM phenotypes of 7 recombinant individuals, which carried only one MG-20 allele at one of the two marker positions, were determined in the F2 generation and the F3 self-progeny. Further co-segregation analysis was performed with the SSR markers TM0060, TM0635 and SSR17, which was predicted from the CM0060 contig sequence by SSRIT (Temnykh et al., 2001). Fluorescence labeled PCR fragments were analysed with an ABI 3730 DNA Analyser and GeneMapper software (Applied Biosystems). Candidate genes within the target region between TM0060 and TM0635 were annotated with GENSCAN (http://genes.mit.edu/GENSCAN.html), BLAST (http://blast.ncbi.nlm.nih.gov/Blast.cgi) and Artemis (Rutherford et al., 2000). All mentioned primers used for this work are listed in Supplemental Table 2.

TILLING

1.2 kb 5' and adjacent 1.4 kb 3' fragments of *NENA* genomic sequence, amplified by the respective primer pairs N-166/167 and N-156/157, were used to perform TILLING of *L. japonicus* as described in (Perry et al., 2003).

Supplemental Discussion

Yeast nucleoporin mutants also show temperature dependent defects. Seh1 is exceptional, as yeast *seh1* null mutants are not affected in mRNA export and can grow at temperatures above 30 °C (Siniossoglou et al., 1996). Nevertheless, *seh1*$^-$ and *nup84*$^-$ are synthetic lethal, as this is the case for any other pair wise combination of knock out alleles of Nup84 subcomplex members (Heath et al., 1995; Goldstein et al., 1996; Siniossoglou et al., 1996). Yeast Nup85•Seh1 and Sec13•Nup145C complexes have similar architectures and interaction of co-expressed Nup85 and Sec13 has been shown (Hsia et al., 2007; Debler et al., 2008). Therefore, structurally homologous SEC13-like 1 or 2, which might assemble with NUP85 during NPC formation in the *nena* mutant background, probably could partially complement a loss of NENA function. Moreover, the stability of the SEC13-like 1 or 2•NUP85 complex might be temperature dependent, causing temperature sensitive symbiotic phenotypes in *nena* mutants. We have tested these hypotheses by yeast two-hybrid analysis performed at 18 °C and 24 °C growth temperature. The results, however, did not support interaction of SEC13 homologs and NUP85 (Supplemental Figure 5A).

Supplemental References

Brohawn, S.G., Leksa, N.C., Spear, E.D., Rajashankar, K.R., and Schwartz, T.U. (2008). Structural evidence for common ancestry of the nuclear pore complex and vesicle coats. Science **322,** 1369-1373.

Debler, E.W., Ma, Y., Seo, H.S., Hsia, K.C., Noriega, T.R., Blobel, G., and Hoelz, A. (2008). A fence-like coat for the nuclear pore membrane. Mol. Cell **32,** 815-826.

Goldstein, A.L., Snay, C.A., Heath, C.V., and Cole, C.N. (1996). Pleiotropic nuclear defects associated with a conditional allele of the novel nucleoporin Rat9p/Nup85p. Mol. Biol. Cell **7,** 917-934.

Heath, C.V., Copeland, C.S., Amberg, D.C., Del Priore, V., Snyder, M., and Cole, C.N. (1995). Nuclear pore complex clustering and nuclear accumulation of poly(A)+ RNA associated with mutation of the *Saccharomyces cerevisiae* RAT2/NUP120 gene. J. Cell Biol. **131,** 1677-1697.

Hsia, K., Stavropoulos, P., Blobel, G., and Hoelz, A. (2007). Architecture of a coat for the nuclear pore membrane. Cell **131,**1313-1326.

Perry, J.A., Wang, T.L., Welham, T.J., Gardner, S., Pike, J.M., Yoshida, S., and Parniske, M. (2003). A TILLING reverse genetics tool and a web-accessible collection of mutants of the legume *Lotus japonicus*. Plant Physiol. **131,** 866-871.

Rutherford, K., Parkhill, J., Crook, J., Horsnell, T., Rice, P., Rajandream, M.A., and Barrell, B. (2000). Artemis: sequence visualization and annotation. Bioinformatics **16,** 944-945.

Schuelke, M. (2000). An economic method for the fluorescent labeling of PCR fragments. Nat. Biotechnol. **18,** 233-234.

Siniossoglou, S., Wimmer, C., Rieger, M., Doye, V., Tekotte, H., Weise, C., Emig, S., Segref, A., and Hurt, E.C. (1996). A novel complex of nucleoporins, which includes Sec13p and a Sec13p homolog, is essential for normal nuclear pores. Cell **84,** 265-275.

Temnykh, S., DeClerck, G., Lukashova, A., Lipovich, L., Cartinhour, S., and McCouch, S. (2001). Computational and experimental analysis of microsatellites in rice (*Oryza sativa* L.): frequency, length variation, transposon associations, and genetic marker potential. Genome Res. **11,** 1441-1452.